FAST-Enabled Controller-Parameter-Parameterized Immittance Transfer Function for Retuning Black-Boxed Inverter-Based Resources

Weihua Zhou, *Senior Member, IEEE*, Alison Murray, Bradley Diverall

***Abstract*—Frequency-domain passivity analysis enables stability screening of black-boxed inverter-based resources (IBRs) directly from measured immittance; however, industrial retuning is often constrained by the lack of a direct mapping from stability-margin targets to controller settings. This letter presents a controller-parameter-parameterized immittance transfer function (CPP-ITF) that represents each immittance element as a rational function whose coefficients are explicit polynomials of a selected tuning parameter. Using a small design-of-experiments (DOE) set (i.e., frequency scans at a few parameter values), the CPP-ITF is identified per frequency and combined with a measured grid-impedance profile to evaluate stability margins over dense parameter grids without additional EMT simulations or scans. Implemented in AEMO's in-house Frequency-domain Admittance-based Stability Tool (FAST) and operationalized via a four-step workflow, the method provides directional tuning guidance and auditable feasibility windows over stability-risk bands. A case study demonstrates accurate prediction of sequence-domain impedance versus the selected tuning parameter, scan-free margin screening across multiple SCRs, and EMT validation at the predicted SCR-dependent critical limits.**

***Index Terms*—Black-box identification, immittance measurement, inverter-based resources, passivity-based stability, controller retuning.**

I. Introduction

THE rapid growth of inverter-based resources (IBRs) in transmission and large distribution networks is reshaping power-system dynamics and shifting stability limits from synchronous-machine electromechanics to converter control interactions [1]. In weak-grid and wide-area settings, these interactions can excite lightly damped or unstable modes over a broad frequency range, and the dominant risk bands may shift with operating point and network strength [2]. Consequently, wideband stability assessment and controller retuning have become routine requirements in connection studies and operational investigations.

In practice, controller retuning is still frequently dominated by time-domain trial-and-error: engineers adjust a subset of gains, rerun EMT simulations, and visually judge whether oscillations are sufficiently damped for each grid condition (e.g., each short-circuit ratio (SCR)) [3]. This process is time-consuming, provides limited quantitative guarantees, and transfers poorly as grid impedance varies. For vendor black-boxed IBRs, immittance scanning is often the only practical route to obtain a frequency-domain representation without access to internal control equations [4]. However, scanning alone primarily reveals *what happens* (frequency responses and passivity/margin indicators), not *what to change*; for owners' engineers and consultants reviewing OEM proposals, translating margin targets into auditable parameter windows still tends to rely on repeated scans or EMT campaigns, which remains costly to operationalize [5].

This letter closes the above gap by introducing a controller-parameter-parameterized immittance transfer function (CPP-ITF) that ties the IBR immittance directly to a selected tuning parameter. Each immittance element at a given frequency is represented as a rational function whose coefficients are explicit polynomials of the chosen parameter and are identified from a small DOE set of immittance measurements taken at a few parameter values. Once identified, the CPP-ITF can be combined with a measured grid-impedance profile to evaluate stability margins over dense parameter grids without additional scans or EMT simulations, yielding directional guidance and auditable feasible intervals over stability-risk bands. The method is embedded in AEMO's in-house FAST tool and aligns with AEMO's frequency-scanning implementations [6].

The key contributions are:

- A per-frequency CPP-ITF identified from a small DOE scan set, preserving compatibility with vendor black-boxing.
- A scan-free retuning procedure that maps margin targets to parameter-feasibility windows by combining the CPP-ITF with measured grid impedance.
- A FAST implementation that operationalizes margin screening into auditable controller retuning for black-boxed IBRs.

The remainder of this letter is organized as follows. Section II describes the observed instability issue and reviews conventional trial-and-error retuning. Section III presents the CPP-ITF synthesis procedure. Section IV demonstrates the proposed method via a representative case study and EMT validation. Section V concludes the letter.

II. Problem Formulation

A. Black-Boxed IBR and Instability Under Weak Grids

Figure 1 shows a single-machine infinite-bus (SMIB) system interfaced with a vendor black-boxed IBR, for which the internal control and circuit implementation are not disclosed. Externally, the IBR is characterized at the point of common

W. Zhou, A. Murray, and B. Diverall are with the Australian Energy Market Operator (AEMO), Melbourne, VIC 3000, Australia (e-mail: weihua.zhou, alison.murray, bradley.diverall@aemo.com.au).

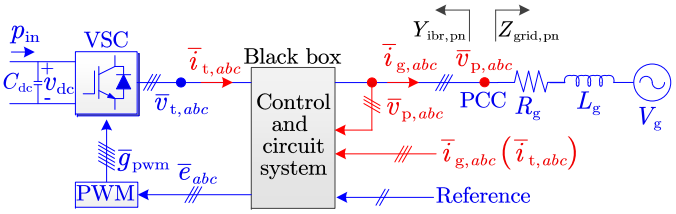

Fig. 1. SMIB configuration with a vendor black-boxed IBR.

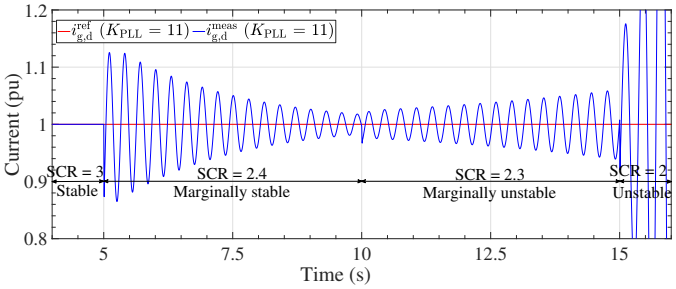

Fig. 2. Active current response under step reductions of SCR ($3 \rightarrow 2.4 \rightarrow 2.3 \rightarrow 2$).

coupling (PCC) by the relationship between PCC voltage and injected current, which can be expressed in the sequence domain as a 2×2 immittance (here, admittance) matrix $\mathbf{Y}_{\text{ibr,pn}}(f)$. The external grid seen from the PCC is represented by an equivalent series impedance $Z_{\text{g}}(s) = R_{\text{g}} + sL_{\text{g}}$ (with fixed $X_{\text{g}}/R_{\text{g}} = 6$ in this study), and the grid strength is characterized by the SCR.

Figure 2 presents PSCAD™/EMTDC™ time-domain results under unity active-current injection and zero reactive-current injection. The plot compares the active current reference and measurement while the SCR is reduced in steps from 3 to 2.4, 2.3, and 2. At $\text{SCR} = 3$, the active current tracks the reference with adequate damping. When the SCR is reduced to 2.4, a low-frequency oscillation is excited and becomes weakly damped (marginally stable). As the SCR is further reduced to 2.3, the oscillation begins to grow (marginally unstable), and at $\text{SCR} = 2$ it diverges rapidly, indicating loss of stability under weak-grid conditions. This motivates controller retuning to maintain adequate stability margins across wide SCRs.

B. Conventional Time-Domain Trial-and-Error Retuning

In current practice, retuning is often performed via time-domain trial-and-error: a selected tuning parameter (here, the PLL gain K_{PLL}) is adjusted and EMT simulations are repeated until the response appears adequately damped for a given SCR. Fig. 3 illustrates this process under weak-grid conditions by overlaying the active current responses obtained with multiple K_{PLL} values. As the grid weakens, higher K_{PLL} settings exhibit poorer damping and may lead to growing oscillations, whereas sufficiently reduced K_{PLL} improves damping and can recover stability. The acceptable K_{PLL} range tightens as SCR decreases, implying that the tuning must be re-identified for each grid condition.

Overall, this approach has two key drawbacks: (i) it does not produce auditable stability margins for tuning certification, and (ii) it transfers poorly across grid-impedance variation,

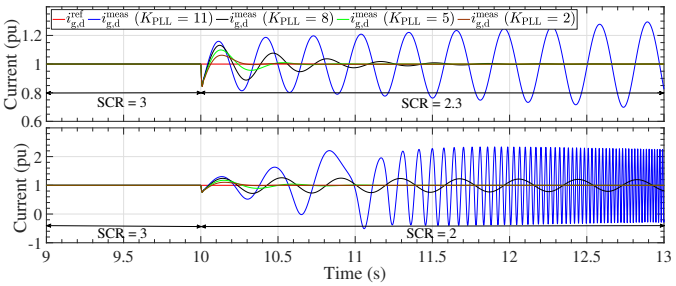

Fig. 3. Conventional time-domain trial-and-error retuning under weak-grid conditions by sweeping K_{PLL}.

requiring repeated EMT iterations as SCR changes. These limitations motivate a scan-efficient, margin-certified method that can rapidly determine feasible tuning windows under varying grid strengths.

III. CPP-ITF Synthesis for Scan-Free Retuning

To translate stability-margin targets into actionable settings for vendor black-boxed IBRs, the measured sequence-domain immittance is modeled as an explicit function of a selected scalar tuning parameter (e.g., PLL, current, or reactive-power-loop gains). Let x denote the tuning parameter (e.g., K_{PLL}), and let $Z_{\alpha\beta}(f;x)$ denote an element of the 2×2 sequence-domain impedance matrix, with $\alpha\beta \in \{\text{pp}, \text{pn}, \text{np}, \text{nn}\}$. At each frequency f, the CPP-ITF approximates each element by a rational function whose coefficients are polynomials of x. For order N,

$$\hat{Z}_{\alpha\beta}(f;x) = \frac{\sum_{n=0}^{N} b_{n,\alpha\beta}(f)\, x^n}{1 + \sum_{n=1}^{N} a_{n,\alpha\beta}(f)\, x^n}, \tag{1}$$

where $a_{0,\alpha\beta}(f) \triangleq 1$ is fixed for normalization. After fitting from only a small DOE scan set, (1) enables scan-free synthesis of $\hat{Z}_{\alpha\beta}(f;x)$ at arbitrary x.

A. Least-Squares Identification of CPP-ITF Coefficients

Assume a DOE data set consisting of M measured scans at controller-parameter values $\{x_m\}_{m=1}^{M}$. For a fixed frequency sample f_i, define the measured data for one element as

$$y_m \triangleq Z_{\alpha\beta}(f_i; x_m), \qquad m = 1, \ldots, M, \tag{2}$$

and define $\mathbf{v}(x) \triangleq [1,\, x,\, x^2,\, \ldots,\, x^N]^{\top}$. Multiplying (1) by its denominator yields a linear equation in the unknown coefficients:

$$y_m \left(1 + \sum_{n=1}^{N} a_{n,\alpha\beta}(f_i)\, x_m^n\right) = \sum_{n=0}^{N} b_{n,\alpha\beta}(f_i)\, x_m^n. \tag{3}$$

Rearranging gives

$$\mathbf{A}_m(f_i)\, \boldsymbol{\theta}_{\alpha\beta}(f_i) = y_m, \qquad m = 1, \ldots, M, \tag{4}$$

where

$$\mathbf{A}_m(f_i) = \left[-y_m x_m^1 \;\cdots\; -y_m x_m^N \;\; 1 \;\; x_m \;\cdots\; x_m^N\right] \in \mathbb{C}^{1\times(2N+1)}$$

and

$$\boldsymbol{\theta}_{\alpha\beta}(f_i) = \left[a_{1,\alpha\beta}(f_i) \;\cdots\; a_{N,\alpha\beta}(f_i)\; b_{0,\alpha\beta}(f_i) \;\cdots\; b_{N,\alpha\beta}(f_i)\right]^{\top}.$$

Stacking (4) over $m = 1, \ldots, M$ yields the complex least-squares problem at frequency f_i:

$$\mathbf{A}(f_i)\,\boldsymbol{\theta}_{\alpha\beta}(f_i) \approx \mathbf{y}(f_i), \tag{5}$$

where $\mathbf{A}(f_i) \in \mathbb{C}^{M\times(2N+1)}$ and $\mathbf{y}(f_i) = [y_1, \ldots, y_M]^\top$. To improve robustness under measurement noise and ill-conditioning, ridge regularization is applied:

$$\boldsymbol{\theta}_{\alpha\beta}(f_i) = \arg\min_{\boldsymbol{\theta}} \|\mathbf{A}(f_i)\boldsymbol{\theta} - \mathbf{y}(f_i)\|_2^2 + \lambda\,\|\boldsymbol{\theta}\|_2^2, \tag{6}$$

with $\lambda \geq 0$. The closed-form solution is

$$\boldsymbol{\theta}_{\alpha\beta}(f_i) = \left(\mathbf{A}^H(f_i)\mathbf{A}(f_i) + \lambda\mathbf{I}\right)^{-1}\mathbf{A}^H(f_i)\mathbf{y}(f_i), \tag{7}$$

where $(\cdot)^H$ denotes the Hermitian transpose. A practical identifiability guideline is $M \geq 2N+1$, matching the number of unknowns in $\boldsymbol{\theta}_{\alpha\beta}(f_i)$. This fitting is performed independently for each frequency f_i and each element $\alpha\beta \in \{\mathrm{pp}, \mathrm{pn}, \mathrm{np}, \mathrm{nn}\}$, using the intersection of frequency samples common to all DOE scans to ensure consistent stacking in (5). The fit quality at each f_i can be summarized via the residual norm (e.g., root-mean-square error) computed from $\|\mathbf{A}(f_i)\boldsymbol{\theta} - \mathbf{y}(f_i)\|_2$.

B. Scan-Free Synthesis and Margin Screening Under Arbitrary Grids

After identification, the impedance element at a new controller setting $x^\star$ is synthesized by direct evaluation of (1):

$$\hat{Z}_{\alpha\beta}(f_i; x^\star) = \frac{\sum_{n=0}^{N} b_{n,\alpha\beta}(f_i)\,(x^\star)^n}{1 + \sum_{n=1}^{N} a_{n,\alpha\beta}(f_i)\,(x^\star)^n}. \tag{8}$$

This yields a synthesized 2×2 sequence-domain impedance matrix $\hat{\mathbf{Z}}(f_i; x^\star)$ over the studied frequency grid without additional scans.

For a selected grid profile $\mathbf{Z}_{\mathrm{grid}}(f)$, FAST combines $\hat{\mathbf{Z}}(f; x^\star)$ with $\mathbf{Z}_{\mathrm{grid}}(f)$ to compute stability indicators (e.g., phase margin) over dense candidate grids of x. Importantly, the screening can return an auditable *feasible tuning window* under each SCR condition rather than a single trial-and-error point.

IV. FAST Implementation and Case Study

A. FAST-Enabled Workflow and DOE Configuration

In FAST, the CPP-ITF retuning workflow is operationalized as:

1) **DOE scans**: acquire a small set of sequence-domain scans at selected controller-parameter values.
2) **CPP-ITF identification**: fit (1) at each frequency and each impedance-matrix element.
3) **Scan-free screening**: synthesize $\hat{\mathbf{Z}}(f; x)$ on dense x grids and compute margins under selected grid profiles/SCRs.
4) **Validation**: confirm critical limits (as needed) via targeted EMT simulations (and/or additional scans).

For the case study, the tuning parameter is the PLL gain K_{PLL}, selected for illustration of the generic CPP-ITF workflow. A DOE set of five measurements is used for identification, with $K_{\mathrm{PLL}} \in \{1, 4, 7, 10, 13\}$. To validate generalization beyond the DOE points, additional measurements at $K_{\mathrm{PLL}} = 3$ and $K_{\mathrm{PLL}} = 9$ are reserved for out-of-sample validation. All files are pre-processed to retain only the common frequency samples across the DOE scans (intersection), ensuring consistent stacking in (5). The CPP-ITF coefficients $\boldsymbol{\theta}_{\alpha\beta}(f_i)$ are then obtained independently for each f_i and each $\alpha\beta \in \{\mathrm{pp}, \mathrm{pn}, \mathrm{np}, \mathrm{nn}\}$ using (6)–(7). The fitted coefficients can be archived and reused to synthesize $\hat{\mathbf{Z}}(f; K_{\mathrm{PLL}})$ at arbitrary K_{PLL} values without repeating scans.

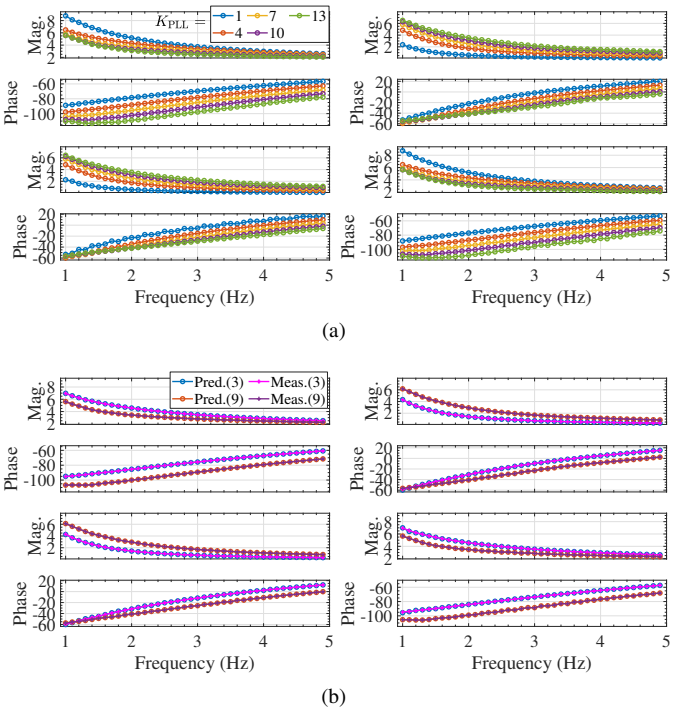

Fig. 4. CPP-ITF synthesis and out-of-sample validation in the sequence domain: (a) measured impedance at DOE points ($K_{\mathrm{PLL}} = 1, 4, 7, 10, 13$); (b) CPP-ITF synthesis at $K_{\mathrm{PLL}} = 3, 9$ with measurement overlays.

B. CPP-ITF Synthesis and Out-of-Sample Validation

Figure 4 summarizes CPP-ITF synthesis and out-of-sample validation in the sequence domain. Fig. 4(a) plots the measured impedance responses at the DOE points ($K_{\mathrm{PLL}} = 1, 4, 7, 10, 13$), which show a consistent dependence on K_{PLL} in both magnitude and phase over the studied band. Using only these DOE scans for identification, the CPP-ITF is evaluated at unseen parameter values via (8). Fig. 4(b) compares the synthesized responses at $K_{\mathrm{PLL}} = 3$ and $K_{\mathrm{PLL}} = 9$ with the corresponding measurements; the predicted curves closely overlay the measured ones for both magnitude and phase. This agreement indicates that the CPP-ITF captures the local mapping $K_{\mathrm{PLL}} \mapsto \mathbf{Z}(f; K_{\mathrm{PLL}})$ with sufficient fidelity for scan-free margin screening.

C. Scan-Free Margin Screening and SCR-Dependent Critical Limits

After CPP-ITF identification, FAST performs scan-free margin screening by evaluating $\hat{\mathbf{Z}}(f; K_{\mathrm{PLL}})$ over a dense grid of candidate K_{PLL} values and combining the synthesized IBR impedance with a selected grid-impedance profile $\mathbf{Z}_{\mathrm{grid}}(f)$.

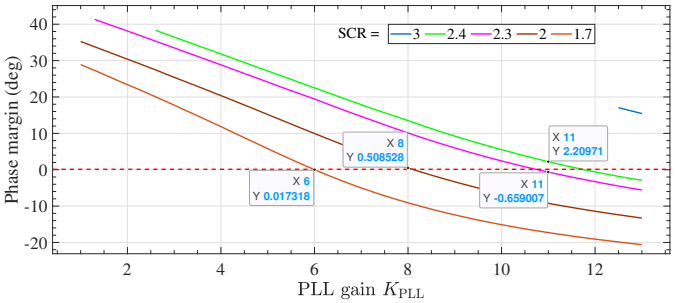

Fig. 5. Scan-free phase-margin screening using the synthesized CPP-ITF: phase margin versus K_{PLL} (swept from 1 to 13 in steps of 0.1) under $\mathrm{SCR} = 3$, 2.4, 2.3, 2, and 1.7.

TABLE I. Comparison of phase margins predicted by the synthesized CPP-ITF and those computed directly from measured immittance data at $K_{\mathrm{PLL}} = 1, 3, 5, 7, 9, 11, 13$ under $\mathrm{SCR} = 3$, 2.4, 2.3, 2, and 1.7.

K_{PLL}	SCR= 3		SCR= 2.4		SCR= 2.3		SCR= 2		SCR= 1.7	
	Pred. PM	Meas. PM	Pred. PM	Meas. PM	Pred. PM	Meas. PM	Pred. PM	Meas. PM	Pred. PM	Meas. PM
1	N/A	N/A	N/A	N/A	N/A	N/A	35.25	35.46	28.89	28.77
3	N/A	N/A	36.46	36.69	33.50	33.11	25.40	25.70	17.73	17.61
5	N/A	N/A	27.15	27.42	24.10	23.75	15.18	15.15	5.79	5.53
7	N/A	N/A	17.88	18.29	14.65	14.82	4.96	5.27	-5.00	-5.32
9	N/A	N/A	9.24	8.67	5.99	5.79	-3.33	-4.24	-12.42	-12.09
11	N/A	N/A	2.21	2.38	-0.66	-0.86	-9.24	-9.86	-17.29	-17.92
13	15.45	15.46	-2.90	-2.18	-5.58	-5.55	-13.30	-12.73	-20.61	-20.47

In this case study, the phase margin is computed at candidate oscillation frequencies identified within the studied band (1–4.9 Hz) via the condition $\mathrm{Im}\{Y_{\mathrm{tot}}(f)\} = 0$, where $Y_{\mathrm{tot}}(f)$ is the total (IBR+grid) admittance formed from the synthesized positive-sequence impedances. If no oscillation frequency is detected in 1–4.9 Hz for a given K_{PLL} and SCR, the phase margin is treated as not defined for that point (yielding blank segments in the phase-margin curves and `N/A` in the tabulated comparisons).

Fig. 5 plots the resulting phase margin as a function of K_{PLL} for $\mathrm{SCR} = 3$, 2.4, 2.3, 2, and 1.7. The phase margin decreases monotonically with increasing K_{PLL}, thereby providing an unambiguous tuning direction. For a given grid strength, the critical retuning point is taken as the largest K_{PLL} that satisfies the prescribed phase-margin requirement (phase margin $= 0^\circ$ corresponds to critical stability). As the grid weakens, the phase-margin curve shifts downward, tightening the admissible upper bound on K_{PLL}. Under the weakest condition, $\mathrm{SCR} = 1.7$, the curve shifts further downward; in particular, maintaining a positive phase margin within 1–4.9 Hz requires $K_{\mathrm{PLL}} \lesssim 6$.

To quantify prediction accuracy against direct calculations from measured scans, Table I compares phase margins predicted by the synthesized CPP-ITF (also used to generate Fig. 5) with those computed directly from measured immittance data at $K_{\mathrm{PLL}} = 1, 3, 5, 7, 9, 11, 13$ under $\mathrm{SCR} = 3$, 2.4, 2.3, 2, and 1.7. Across all cases where an oscillation frequency is detected within 1–4.9 Hz, the predicted and measured phase margins exhibit close agreement, confirming that the CPP-ITF provides an accurate surrogate for scan-free margin screening within the proposed workflow.

D. EMT Validation of the $\mathrm{SCR} = 1.7$ Critical Limit

Figure 6 shows EMT time-domain results for $\mathrm{SCR} = 1.7$ as the PLL gain is increased from $K_{\mathrm{PLL}} = 5.5$ to 6 and 6.5.

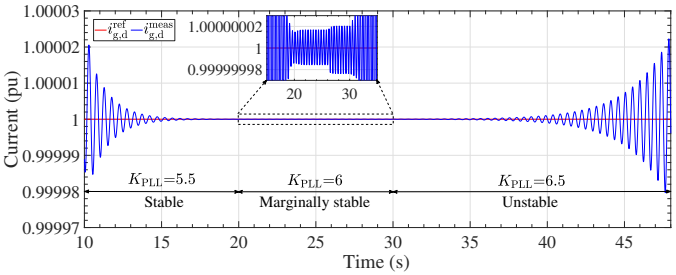

Fig. 6. EMT validation of the CPP-ITF-predicted critical PLL tuning limit under $\mathrm{SCR} = 1.7$.

With increasing K_{PLL}, the effective damping deteriorates and the oscillatory response becomes progressively less stable: the response remains acceptably damped at $K_{\mathrm{PLL}} = 5.5$, becomes marginal at $K_{\mathrm{PLL}} = 6$, and turns unstable at $K_{\mathrm{PLL}} = 6.5$. These EMT results confirm that $K_{\mathrm{PLL}} \approx 6$ is the appropriate critical value for $\mathrm{SCR} = 1.7$, thereby validating the stability-threshold prediction in Fig. 5.

V. Conclusion

This letter presented a FAST-embedded retuning workflow for vendor black-boxed IBRs based on frequency-scan data. The proposed CPP-ITF surrogate enables scan-free synthesis of sequence-domain immittance and rapid stability-margin screening over dense controller-parameter grids from a small DOE set. The case study demonstrates that the synthesized impedance trends and the resulting margin predictions are consistent with those obtained from measured scans, and that targeted EMT simulations corroborate the SCR-dependent critical tuning limits identified by the proposed screening process. Overall, the CPP-ITF provides a practical and auditable path from stability-margin targets to controller-parameter feasibility windows without repeated scanning campaigns. Future work will extend the framework to multi-parameter retuning and operating-envelope CPP-ITFs, enabling wide-spectrum tuning practice and demonstrations beyond PLL gains.

References

[1] Y. Cheng, L. Fan, J. Rose, S.-H. Huang, J. Schmall, X. Wang, X. Xie, J. Shair, J. R. Ramamurthy, N. Modi *et al.*, "Real-world subsynchronous oscillation events in power grids with high penetrations of inverter-based resources," *IEEE Trans. Power Syst.*, vol. 38, no. 1, pp. 316–330, Jan. 2023.

[2] N. Modi, E. M. Farahani, A. Jalali, J. Ramamurthy, C. Chin, and B. Soetantijo, "Replication of real-world sub-synchronous oscillations in inverter-based resources dominated grid," *IEEE Trans. Power Del.*, vol. 39, no. 3, pp. 1399–1406, Jun. 2024.

[3] "Model acceptance test guideline," Australian Energy Market Operator (AEMO), Feb. 2021. [Online]. Available: https://www.aemo.com.au/-/media/files/electricity/nem/network_connections/model-acceptance-test-guideline-feb-2021.pdf

[4] J. Sun, "Impedance-based stability criterion for grid-connected inverters," *IEEE Trans. Power Electron.*, vol. 26, no. 11, pp. 3075–3078, Nov. 2011.

[5] W. Zhou, N. Mohammed, and B. Bahrani, "Operating-point parameterized state-space models of black-boxed grid-following inverters for maximum transferable active power prediction," *IEEE Trans. Ind. Electron.*, vol. 71, no. 12, pp. 16882–16887, Dec. 2024.

[6] "Frequency scanning," Australian Energy Market Operator (AEMO). [Online]. Available: https://www.aemo.com.au/energy-systems/electricity/national-electricity-market-nem/participate-in-the-market/network-connections/connection-resources/focus-areas-and-initiatives/frequency-scanning